FULL PAPER

Self-Assembled, Millimeter-Sized TIPS-Pentacene Spherulites Grown on Partially Crosslinked Polymer Gate Dielectric

Hocheon Yoo, Hyun Ho Choi, Tae Joo Shin, Taiuk Rim, Kilwon Cho, Sungjune Jung,* and Jae-Joon Kim**

Here, a highly crystalline and self-assembled 6,13-bis(triisopropylsilyleth ynyl) pentacene (TIPS-Pentacene) thin films formed by simple spin-coating for the fabrication of high-performance solution-processed organic field-effect transistors (OFETs) are reported. Rather than using semiconducting organic small-molecule–insulating polymer blends for an active layer of an organic transistor, TIPS-Pentacene organic semiconductor is separately self-assembled on partially crosslinked poly-4-vinylphenol:poly(melamine-*co*-formaldehyde) (PVP:PMF) gate dielectric, which results in a vertically segregated semiconductor-dielectric film with millimeter-sized spherulite-crystalline morphology of TIPS-Pentacene. The structural and electrical properties of TIPS-Pentacene/PVP:PMF films have been studied using a combination of polarized optical microscopy, atomic force microscopy, 2D-grazing incidence wide-angle X-ray scattering, and secondary ion mass spectrometry. It is finally demonstrated a high-performance OFETs with a maximum hole mobility of 3.40 $cm^2 V^{-1} s^{-1}$ which is, to the best of our knowledge, one of the highest mobility values for TIPS-Pentacene OFETs fabricated using a conventional solution process. It is expected that this new deposition method would be applicable to other small molecular semiconductor–curable polymer gate dielectric systems for high-performance organic electronic applications.

1. Introduction

Organic field-effect transistors (OFETs) based on solution-processable organic semiconductors have been investigated over the last decade targeting soft electronics application.[1–5] Among the solution-processable organic semiconductors, small molecular semiconductors such as 6,13-bis(triisopropylsilylethynyl) pentacene (TIPS-Pentacene)[6–10] and difluoro-bis(triethylsilylethynyl) anthradithiophene (diF-TES-ADT)[11–14] have attracted much attention because of their relatively high field-effect mobility and solution processability. One way to further improve performance characteristics of the small-molecule OFET devices is to blend the semiconducting materials with one or more insulating polymer materials.[11,15] Initially investigated by Sirringhaus and co-workers that used a two-component blend based on polythiophenes and different insulating polymers for OFET applications,[16] this approach has been also applied successfully to small-molecule organic semiconductors,[11] blended with insulating[17–20] or other semiconducting polymers.[21] Recently, high mobility OFETs have been demonstrated with a TIPS-Pentacene blend[9] and with a diF-TES-ADT blend.[13]

Because charge carriers in OFETs are mostly transported in a direction parallel to the substrate, the formation of a vertically phase-separated bilayer structure can lead to higher performances of the transistors. Factors such as the surface tension of each component,[19] the solvent evaporation rate,[9] molecular weight of insulating polymer,[22] and the characteristics of the substrate[23,24] should be considered for the sharp vertical phase separation, so the choice of adequate insulating polymers is quite limited and the postannealing processes are sometimes needed.[20,22,23] Furthermore, there is inevitably the intermixed area with thickness of tens to hundreds of nanometers between semiconductor and insulating polymer layers. This will presumably result in the rough conduction channel if the interface between semiconductor and insulating polymer is used as a conduction channel (interface channel), so the carrier mobilities become lower than ideal values. For this reason, a strategy to use polymers only as a template and to use the opposite semiconducting side from the interface as a conduction channel (top channel) has been suggested.[11] Kippelen and co-workers reported that the top channel exhibited the 2.0–4.7 times higher mobilities than the interface channel in the case of TIPS-Pentacene OFETs.[9]

H. Yoo, Dr. T. Rim, Prof. S. Jung, Prof. J.-J. Kim
Department of Creative IT Engineering
Pohang University of Science and Technology (POSTECH)
Pohang 790-784, Korea
E-mail: sjjung@postech.ac.kr; jaejoon@postech.ac.kr
Dr. H. H. Choi, Prof. K. Cho
Department of Chemical Engineering and
Center for Advanced Soft Electronics (CASE)
Pohang University of Science and Technology (POSTECH)
Pohang 790-784, Korea
E-mail: kwcho@postech.ac.kr
Prof. T. J. Shin
UNIST Central Research Facilities & School of Natural Science
UNIST
Ulsan 689-798, Korea

DOI: 10.1002/adfm.201501381

However, the device using top channel must have the additive fabrication of gate dielectric layer, so there is a limited choice of processing solvents for depositing gate dielectric to avoid the dissolution of small molecular semiconductors.

Here, we report highly crystalline and self-assembled TIPS-Pentacene thin films formed by simple spin-coating for the fabrication of high-performance solution-processed OFETs. Rather than mixing two organic components before depositing a film as used in all the previous studies, we process TIPS-Pentacene organic semiconductor separately on partially crosslinked poly-4-vinylphenol:poly(melamine-*co*-formaldehyde) (PVP:PMF) gate dielectric, which results in a vertically segregated film with millimeter-sized spherulite-crystalline morphology of TIPS-Pentacene. The structural and electrical properties of TIPS-Pentacene/PVP:PMF films have been studied using a combination of polarized optical microscopy (POM), atomic force microscopy (AFM), 2D-grazing incidence wide-angle X-ray scattering (2D-GIWAXS), and secondary ion mass spectrometry (SIMS). We finally demonstrate a high-performance OFETs with a maximum hole mobility of 3.40 $cm^2 V^{-1} s^{-1}$ which is, to the best of our knowledge, one of the highest mobility values for TIPS-Pentacene OFETs fabricated using conventional solution processes.

2. Results and Discussion

Figure 1 is the schematic of our experimental system that shows the formation process of a small molecular semiconductor thin film. We prepared TIPS-Pentacene in 1,2-dichlorobenzene solvent and partially crosslinked PVP:PMF (pc-PVP:PMF) thin films. The degree of crosslinking of PVP:PMF layer can be tuned by duration and temperature of thermal annealing. In contrast to conventional fully crosslinked PVP:PMF (FC-PVP:PMF),[26–28] we expect that organic solvents can diffuse through the relatively loose network of pc-PVP:PMF, which causes enough swelling for TIPS-Pentacene molecules to permeate. After the TIPS-Pentacene solution is dropped onto pc-PVP:PMF layer for spin coating, the intermixed layer of tri-components (TIPS-Pentacene, solvent, and pc-PVP:PMF) is formed within a few seconds right after solution dropping (Figure 1, Step A). After starting the spinning, the solution droplet is first removed by centrifugal force and a part of TIPS-Pentacene is quickly solidified. Next, the permeated TIPS-Pentacene solution spontaneously moves to the top pc-PVP:PMF surface by the concentration gradient (Figure 1, Step B). In this step, the permeated TIPS-Pentacene and solvent molecules are expected to help the growth and assembly of solid-state TIPS-Pentacene layers.

The electrical characteristics of the fabricated thin films were evaluated with the top-contact bottom-gate OFETs (**Figure 2**a). TIPS-Pentacene and PVP:PMF were used as semiconductor and gate dielectric, respectively, and 94% out of the 30–35 fabricated devices exhibited the prominent OFET performances. Figure 2b shows the typical transfer characteristic of TIPS-Pentacene OFETs with the optimized pc-PVP:PMF layer. The device was operated in the saturation regime with gate voltage varying from 10 to −40 V and source/drain voltage fixed at 0 /−40 V, respectively. The gate leakage was a few nA and the on/off ratio was over 10^4. The on-set and threshold voltage were below −10 V. The histograms of hole mobility and current on/off ratio for the devices fabricated under the optimized condition are presented in Figure 2c. Most devices exhibited hole mobilities above 1 $cm^2 V^{-1} s^{-1}$. The average and maximum hole mobilities were 2.07 and 3.40 $cm^2 V^{-1} s^{-1}$, respectively.

This high value of hole mobility has not been measured when PVP:PMF layer is fully crosslinked,[26–28] which implies that pc-PVP:PMF allows the permeation of solvent and TIPS-Pentacene unlike fully crosslinked PVP:PMF and affects the microstructure of TIPS-Pentacene layer. To verify it, we investigated how the degree of crosslinking in pc-PVP:PMF affects the growth of TIPS-Pentacene layer and resultant OFET

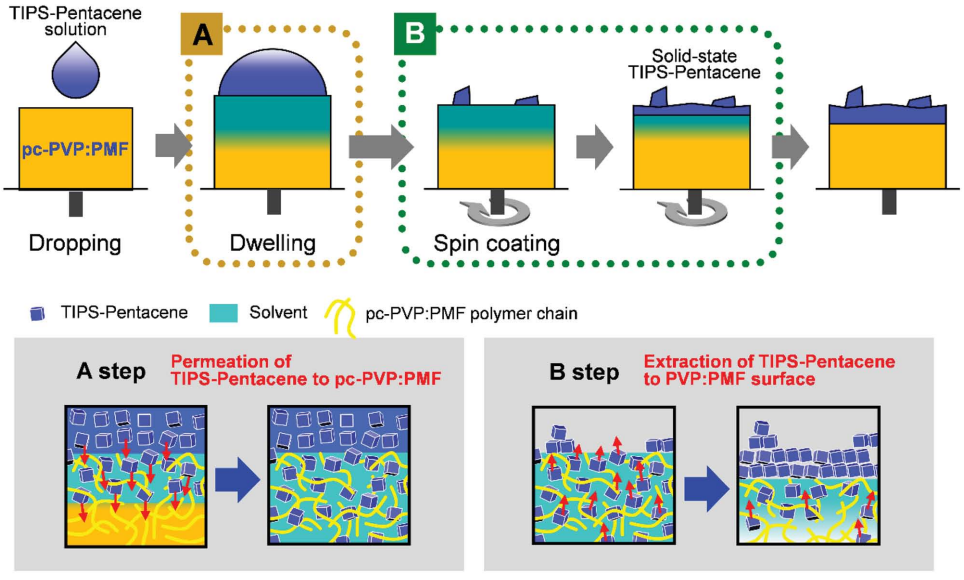

Figure 1. Schematic illustration of formation dynamics of crystalline TIPS-Pentacene layer in this experiment. pc-PVP:PMF: partiallycrosslinked PVP:PMF. Dwelling time: time interval between solution dropping and spinning.

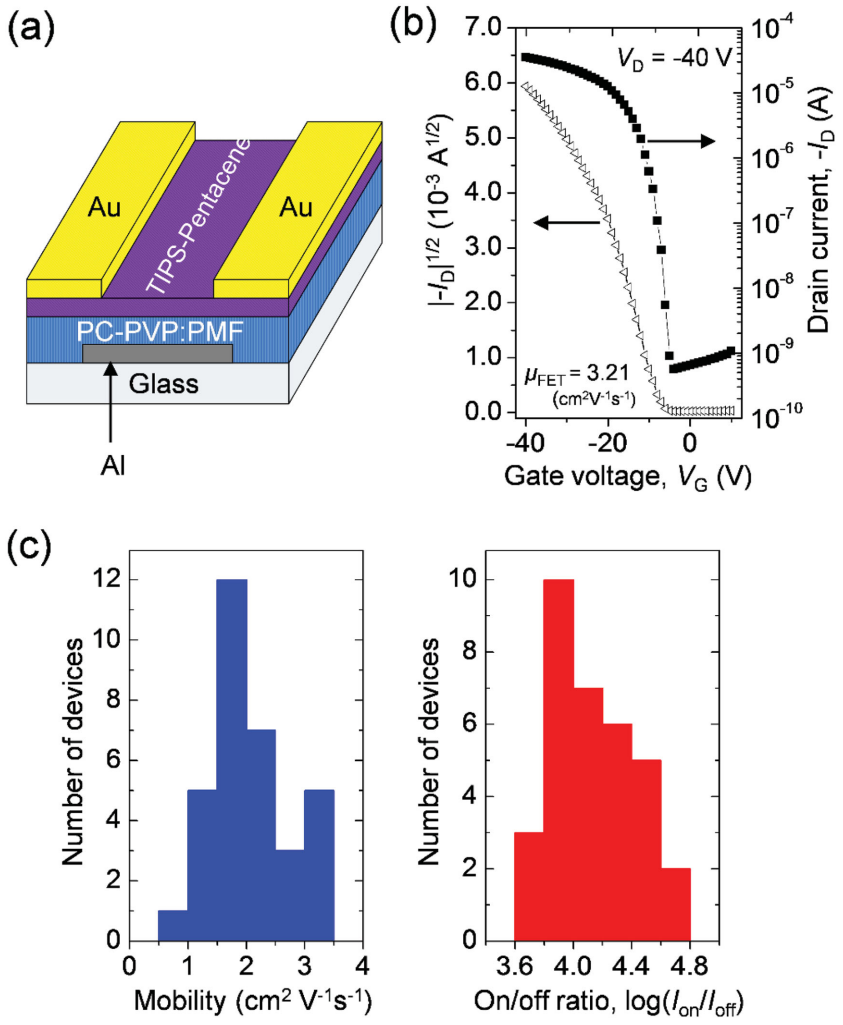

Figure 2. a) Device structure of TIPS-Pentacene/pc-PVP:PMF-based OFETs. b) Transfer characteristic curve and c) histogram of field-effect mobility (left) and on/off ratio (right) for the devices fabricated under the optimized condition.

performances (**Figure 3**). The degree of crosslinking of a PVP:PMF film increased by extending the duration of thermal annealing (10, 15, 20, 25, and 30 min). The surface energy of the PVP:PMF layer decreased from 60.1 down to 43.8 mJ m^{-2} as the annealing time increased, which resulted in the termination of hydrophilic alkoxy groups by condensation reaction.[29,30] POM image revealed that TIPS-Pentacene molecules were solidified into spherulitic crystallites on the pc-PVP:PMF surface in the samples II and III (**Figure 4**a). The angle-dependent POM images confirm the homogeneously distributed spherulite grains (Figure 4b,c). The radius of these spherulites was submillimeter, which means one or two spherulites cover the conduction channel (width: 1500 μm and length: 100 μm), so the intraspherulite charge transport is the dominant conduction mechanism in these samples.

TIPS-Pentacene molecules were crystallized into large-sized spherulites at an optimized degree of PVP:PMF crosslinking, while the spherulitic morphologies did not appear when the degree of crosslinking was relatively low (sample I) or high (samples IV and V). We believe that at the optimized degree (samples II and III), the semiconductor and solvent molecules could permeate into the PVP:PMF layer without significantly affecting the polymer–polymer network. However, when PVP:PMF layer is poorly crosslinked (sample I), it contains a number of uncured polymeric chains, which can be dissolved by solvent and be blended with TIPS-Pentacene solution. These blended PVP and PMF chains hindered the spherulitic growth of TIPS-Pentacene molecules. For the case of samples IV and V where PVP:PMF layer is highly or fully crosslinked, the permeation of TIPS-Pentacene solution into PVP:PMF layer is blocked due to the densely bounded polymeric network, and the segregation and precipitation of TIPS-Pentacene from PVP inside to surface do not arise. Moreover, the surface energy of PVP:PMF layer decreased with the increase of the degree of crosslinking, which resulted in the thin-film dewetting as shown in POM images. Therefore, the optimized crosslinking of PVP:PMF allowed the permeation and extraction of TIPS-Pentacene solution with adequate degree for TIPS-Pentacene to be self-assembled and rearranged.

Depth profile SIMS analysis was used to evaluate the extent of vertical TIPS-Pentacene phase segregation for correlation with the POM analysis. TIPS-Pentacene and PVP:PMF contain silicon and nitrogen atoms, respectively, so the variations with ion-milling depth in the silicon and nitrogen signals were monitored (**Figure 5**a). When PVP:PMF was uncured, the silicon and nitrogen signals increased together,

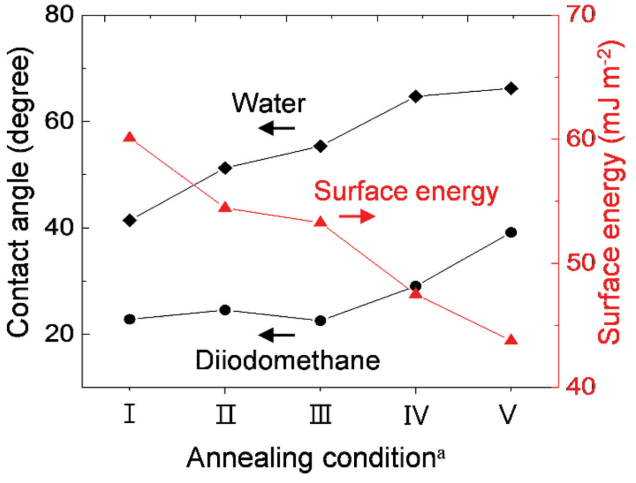

Figure 3. Contact angle and surface energy values as a function of annealing condition.

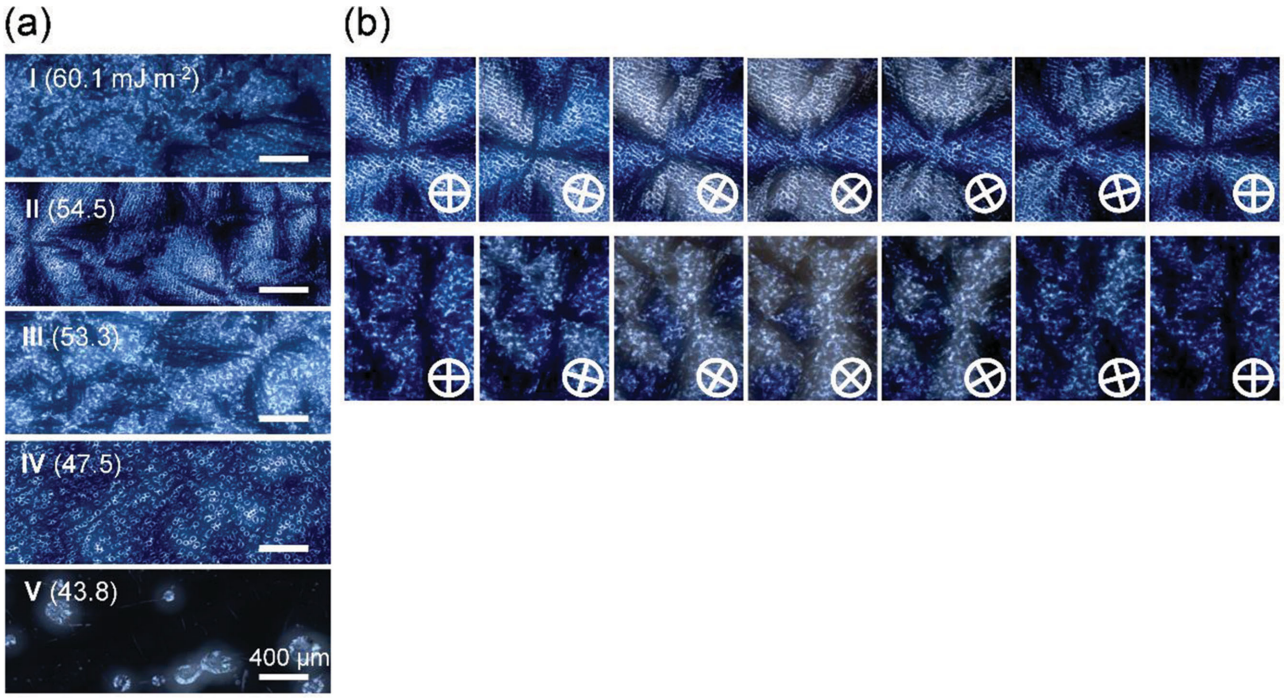

Figure 4. a) Microstructure of TIPS-Pentacene OFETs as a function of curing time for PVP:PMF layer (I: 10 min, II: 15 min, III: 20 min, IV: 25 min, and V: 30 min). b) Polarized optical microscopic (POM) images of TIPS-Pentacene layers. The inset quantitative values: a) PVP:PMF surface energy and b) polarization angle of the incident light (0° to 90°) in the optimal curing conditions (II and III).

implying that the blend film of TIPS-Pentacene and PVP:PMF was formed. The samples II and V in which PVP:PMF was partially or fully cured exhibited the sharp silicon signal near surface (0–100 nm for sample II and 0–70 nm for sample V). This silicon signal weakened abruptly below this layer, while the nitrogen signal strengthened. In addition, the decreasing tendencies of silicon signals in the samples II and V were similar to each other. It implies that the sample II formed the vertically phase-separated TIPS-Pentacene(top)/PVP:PMF(bottom) bilayer structure with a sharp interface. We found that this bilayer structure could not be achieved and the blend film was formed when the spinning time was quite short (Figure 5d). This indicates that the permeation of TIPS-Pentacene solution into pc-PVP:PMF is spontaneous, but the centrifugal force by spinning conversely promotes the extraction of TIPS-Pentacene solution onto pc-PVP:PMF surface.

The variations in device performances with increasing surface energy of a PVP:PMF layer are summarized in **Figure 6**a,b and **Table 1**. Devices with the largest spherulitic grains (sample II) exhibited the highest hole mobilities. This indicates that intraspherulite charge transport is the most facile. This spherulitic morphologies have been frequently observed in high-performance small molecular OFETs.[11,30] Loo and coworkers observed that this intraspherulitic charge transport is independent of the general direction of π-stacking because of low-angle domain boundaries within single spherulite.[30] Furthermore, this low crystallographic misorientation allows faster intermolecular charge transport than high crystallographic misorientation that is frequently observed at the spherulite grain boundary. Therefore, the devices with submillimeter-sized spherulites exhibited the highest mobilities regardless of how their channels are oriented with respect to the general π-stacking direction. To further study the growth of TIPS-Pentacene spherulites, we changed the amount of permeated TIPS-Pentacene solution by varying dwell time (time interval between solution dropping and spinning) from 0.1 to 10 s, leaving the degree of PVP:PMF crosslinking unchanged. The pc-PVP:PMF with surface energy of 54.5 mJ m^{-2} (sample II) was used as gate dielectric.

All samples exhibited the spherulitic morphologies of TIPS-Pentacene layers as shown in POM images, but the size of spherulitic grains were significantly different (**Figure 7**a). The distance from spherulite center to its edge as a radius of spherulitic grains increased from 160 to 511 μm on average with increasing dwell time from 0.1 to 10 s, as shown in Figure 7d. The coherence length of crystalline domains was also dependent on the dwell time. Figure 7b shows 2D-GIWAXS patterns of TIPS-Pentacene/pc-PVP:PMF films with dwell times of 0.1 and 10 s. Both films exhibited strong (00*l*) diffraction peaks of TIPS-Pentacene along out-of-plane, but the full width at half maximum (FWHM) was much larger for the sample with 0.1 s dwell time (0.0142 $Å^{-1}$) than for the sample with 10 s dwell time (0.0089 $Å^{-1}$) (Figure 7c). Consequently, the calculated coherence length of TIPS-Pentacene crystalline domains was longer for the sample with 10 s dwell time (63.7 nm) than for the sample with 0.1 s dwell time (39.8 nm). Both POM and 2D-GIWAXS results indicate that the amount of permeated TIPS-Pentacene solution determines the size of crystalline grains. From the aforementioned SIMS analysis, we verified that the permeated TIPS-Pentacene molecules are slowly

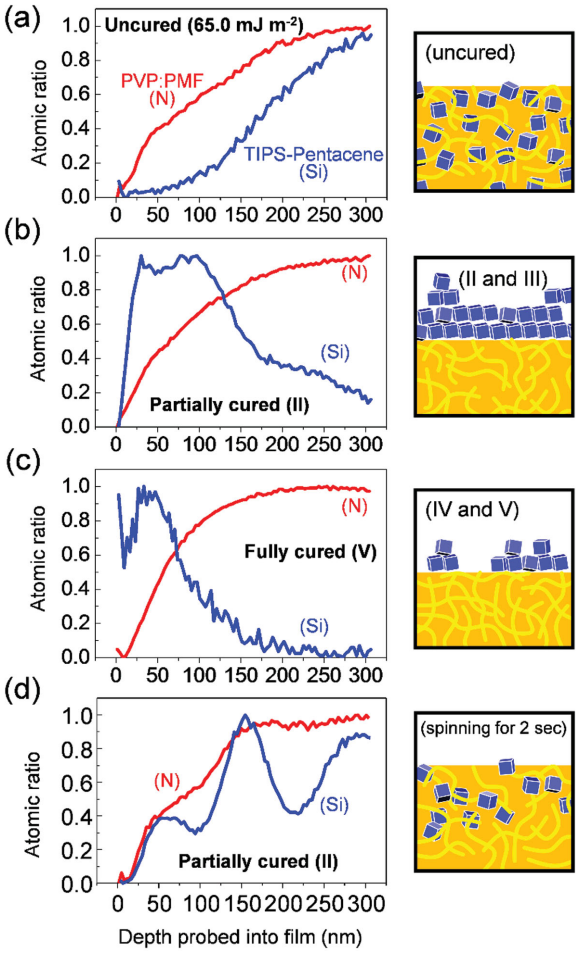

Figure 5. Secondary ion mass spectrometry (SIMS) depth profiles of Si (TIPS-Pentacene) and N (PVP:PMF) as a function of the degree of crosslinking (left) with a) no curing, b) II, c) V, and d) II with decreased spinning time (2 s, 5000 rpm). Respective schematic vertical structures are shown on the right side of each SIMS profile.

and continuously segregated onto pc-PVP:PMF surface in the spinning step due to the reduced miscibility by solvent evaporation. In this procedure, we believe that the evaporation of solvent promotes self-assembly and/or rearrangement of solid-state TIPS-Pentacene, and the migrating TIPS-Pentacene molecules are crystallized below preformed TIPS-Pentacene layer. It was observed that device mobility was significantly improved from 0.33 (average: 0.19 $cm^2 V^{-1} s^{-1}$) to 3.40 $cm^2 V^{-1} s^{-1}$ (average: 2.07 $cm^2 V^{-1} s^{-1}$) due to the increase in spherulite sizes, as the dwell time increased in Figure 7e. There was an almost linear relationship between hole mobilities and radius of spherulitic grains as seen in Figure 7f. It is because the portion of interspherulite charge transport decreases with the increase of spherulite size. When the dwell time is above 10 s, both radius of spherulitic grains and hole mobilities were saturated.

In our system, the intermixed layer of tri-molecules resulting from the permeation of TIPS-Pentacene solution into pc-PVP:PMF layer resembles the phase of TIPS-Pentacene/PVP:PMF blend solution. However, the swollen pc-PVP:PMF distinctly maintains its crosslinked network form unlike conventional blend systems. Hence, in the spinning step, only TIPS-Pentacene solution emerges onto pc-PVP:PMF surface and TIPS-Pentacene/pc-PVP:PMF bilayer structure with sharp interface can be easily achieved without any cumbersome post-process. It is considered that the solvent extraction onto pc-PVP:PMF surface is slow enough for the permeated solvent to deliver TIPS-Pentacene solute to the surface and to help self-assembly of TIPS-Pentacene molecules. As a result, TIPS-Pentacene crystalline grains with the larger size than the dimension of the OFET device were achieved.

3. Conclusion

In summary, we demonstrate a highly crystalline, uniform, and isotropic thin films of a small molecular semiconductor formed by a simple spin-coating method. The partial crosslinking of polymer gate-dielectrics allows the organic semiconductor in a solvent to permeate into it while maintaining its complex network even after the solvent evaporation. Experimentally, we found that the degree of crosslinking in pc-PVP:PMF affected the permeation and extraction of TIPS-Pentacene molecule in pc-PVP:PMF network. The permeation of TIPS-Pentacene solution into pc-PVP:PMF is spontaneous during dwelling, and then the solvent evaporation during spinning promotes the extraction of TIPS-Pentacene solution onto pc-PVP:PMF surface. The residual solvent in pc-PVP:PMF network evaporates slowly, so it helps the self-assembly of TIPS-Pentacene molecules. For this reason, the size of crystalline TIPS-Pentacene grains increases with the amount of permeated TIPS-Pentacene solution, and finally grows to the millimeter size under an optimized condition. As a result, the TIPS-Pentacene layers had millimeter-sized spherulitic morphologies and their device consequently exhibited high FET mobilities with maximum value of 3.40 $cm^2 V^{-1} s^{-1}$. We expect that this new deposition method would be applicable to other small molecular semiconductor–curable polymer gate dielectric systems for high-performance organic electronic applications.

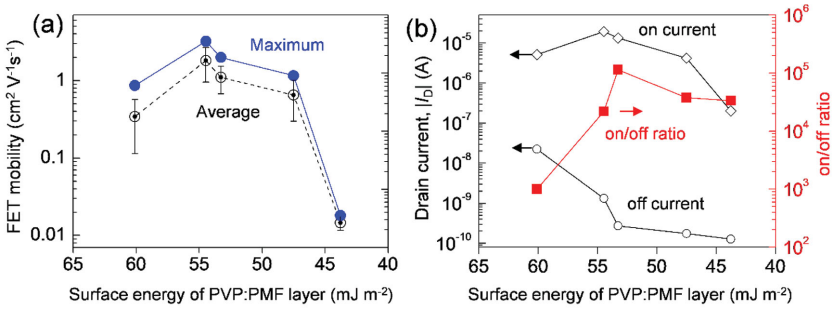

Figure 6. Electrical performances of TIPS-Pentacene OFETs as a function of curing time for PVP:PMF layer (I: 10 min, II: 15 min, III: 20 min, IV: 25 min, and V: 30 min). a) FET mobility and b) on and off drain currents and on/off ratio as a function of surface energy of PVP:PMF layer.

Table 1. Summary of the OFET performances as a function of PVP:PMF annealing duration.

	Annealing time[a)] [min]	Mobility [$cm^2 V^{-1} s^{-1}$]		On/off ratio		$I_{on}^{average}$ [μA]	$I_{off}^{average}$ [nA]	Capacitance [$nF\ cm^{-2}$]
		Average	Maximum	Average	Maximum			
I	10	0.34	0.86	1.0×10^3	4.0×10^3	−5.1	−22.5	3.93
II	15	2.07	3.40	1.7×10^4	6.2×10^4	−20.0	−1.3	3.15
III	20	1.52	2.93	5.8×10^4	2.3×10^5	−13.3	−0.3	2.76
IV	25	0.65	1.16	3.8×10^4	7.8×10^4	−4.2	−0.2	2.61
V	30	0.015	0.018	3.3×10^4	1.5×10^5	−0.2	−0.1	2.06

[a)] I–III: 100 °C; IV: 100 °C (20 min) + 150 °C (5 min); V: 100 °C (20 min) + 150 °C (10 min).

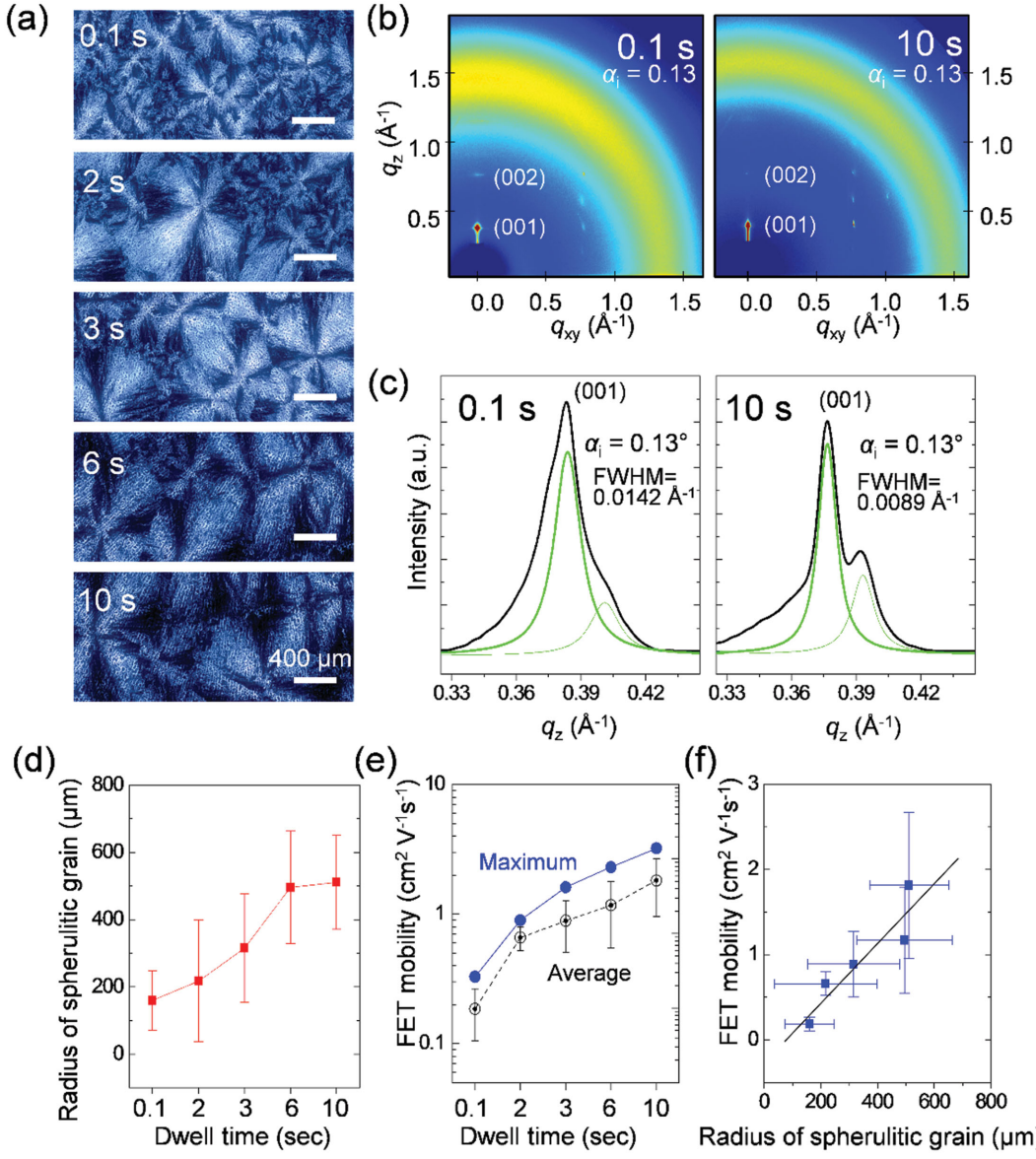

Figure 7. Microstructure and electrical properties of TIPS-Pentacene OFETs as a function of dwell time, i.e., time interval between TIPS-Pentacene solution dropping and spinning. a) POM images of TIPS-Pentacene layers. b) 2D-grazing wide-angle X-ray scattering patterns and c) (001) diffraction peak profiles in out-of-plane. Dependence of d) spherulitic grain size and e) FET mobility on the dwell time. Radius of spherulitic grain: the distance from spherulite center to its edge. f) The relationship between the spherulitic grain size and FET mobility.

4. Experimental Section

Materials: TIPS-Pentacene with a purity of >99.9% from Ossila was used without further purification. We used PVP ($Mw \approx 22\,000$) and PMF ($Mn \approx 432$) from Sigma-Aldrich. Glass substrate (Eagle-XG, Corning) was used after cleaning in an ultrasonic bath with deionized water, acetone, and isopropanol for 10 min, respectively.

Device Fabrication: The top-contact bottom-gate OFETs were fabricated on glass substrate. All steps were conducted in a N_2-purged glove box. The patterned aluminum and gold were used as gate and source/drain, respectively. The channel width and length are 1500 and 100 μm, respectively. The 56 wt% of PVP:PMF (1:5 weight ratio) in propylene glycol methyl ether acetate (PGMEA) was spin-coated on the gate-patterned glass substrate (3000 rpm for 80 s). The thickness of the casted PVP:PMF layers was ~2 μm. These films were partially or fully cured by thermal annealing; I–III: 100 °C (10–20 min); IV: 100 °C (20 min) + 150 °C (5 min); V: 100 °C (20 min) + 150 °C (10 min). Next, the 1 wt% of TIPS-Pentacene in 1,2-dichlorobenzene was spin-coated on pc-PVP:PMF or FC-PVP:PMF (2500 rpm for 80 s). In this step, dwell time was controlled from 0.1 to 10 s. Finally, gold electrodes were thermally deposited through metal shadow mask.

Electrical Characterization: The current–voltage and capacitance–voltage curves were measured using semiconductor analyzer (Agilent 4156C) and LCR meter (E4980A) in ambient environment. Metal-insulator-semiconductor-metal (MISM) structure was used to obtain accurate capacitances. In the capacitance–voltage measurement, the applied gate voltage was from −10 to −20 V, at which the OFET devices accumulated the conductive hole channel and the saturation mobilities were calculated (Figure S2, Supporting Information).

Microstructural Characterization: 2D-GIWAXS measurement was conducted at PLS-II 9A U-SAXS beamline of Pohang Accelerator Laboratory in Korea. The X-rays coming from the in-vacuum undulator are monochromated ($\lambda = 1.120$ Å) using a double-crystal monochromator and are vertically and horizontally focused (300 (H) × 30 (V) μm^2 in FWHM @ sample position) using K-B type mirrors. Vacuum 2D-GIWAXS system is equipped with a 7-axis-motorized sample stage for the fine alignment of thin film. The incidence angle of X-ray beam was set to 0.13°, which is just above the critical angle of TIPS-Pentacene. GIXD patterns were recorded with a 2D CCD detector (Rayonix SX165, USA) and X-ray irradiation time was 10 s. Diffraction angles were calibrated by a precalibrated sucrose (Monoclinic, P21, a = 10.8631 Å, b = 8.7044 Å, c = 7.7624 Å, β = 102.938°) and the sample-to-detector distance was about 225.6 mm. The morphologies of TIPS-Pentacene layers were analyzed using POM (Carl Zeiss) and AFM (Veeco Dimension 3100 and Nanoscope V (Version 7.0)). The depth profile analysis was carried out by using dynamic SIMS 6F instrument (IMS 6F, CAMECA, France) equipped with O_2^+ ion guns. O_2^+ ion was used as primary ion with voltage and current of 12.5 kV and 200 nA, respectively. The raster size was over 200 μm × 200 μm. In this experiment, we choice mass resolution ($m/\Delta m$) of above 10^3 because $14N^+$ and $28Si^{2+}$ ion signals could be separated from main peak in this range. The thickness of the PVP:PMF layers was measured by the surface profilometer (DektakXT) after dissolving the semiconductor layer by 1,2-dichlorobenzene solvent. Every sample was fully cured before dissolving the semiconductor layer in order to protect the PVP:PMF layers from any impact by the solvent.

Supporting Information

Supporting Information is available from the Wiley Online Library or from the author.

Acknowledgements

H.Y. and H.H.C. equally contributed to this work. This work was in part supported by the MSIP (Ministry of Science, ICT, and Planning), Korea under the "IT Consilience Creative Program" (IITP-2015-R0346-15-1007) supervised by IITP(Institute for Information & communications Technology Promotion) and in part by a grant (Code No. 2011-0031628 and 2014M3A6A5060952) from the Center for Advanced Soft Electronics under the Global Frontier Research Program of the Ministry of Science, ICT & Future Planning, Korea.

Received: April 7, 2015
Published online: May 7, 2015

[1] Y.-Y. Noh, N. Zhao, M. Caironi, H. Sirringhaus, *Nat. Nanotechnol.* **2007**, *2*, 784.
[2] G. Schwartz, B. C.-K. Tee, J. Mei, A. L. Appleton, D. H. Kim, H. Wang, Z. Bao, *Nat. Commun.* **2013**, *4*, 1859.
[3] A. Van Breemen, T. Zaba, V. Khikhlovskyi, J. Michels, R. Janssen, M. Kemerink, G. Gelinck, *Adv. Funct. Mater.* **2014**, *25*, 278.
[4] L. Zhang, N. S. Colella, B. P. Cherniawski, S. C. B. Mannsfeld, A. L. Briseno, *ACS Appl. Mater. Interfaces* **2014**, *6*, 5327.
[5] A. Sou, S. Jung, E. Gili, V. Pecunia, J. Joimel, G. Fichet, H. Sirringhaus, *Org. Electron.* **2014**, *15*, 3111.
[6] S. K. Park, T. N. Jackson, J. E. Anthony, D. A. Mourey, *Appl. Phys. Lett.* **2007**, *91*, 063514.
[7] B. K. C. Kjellander, W. T. T. Smaal, J. E. Anthony, G. H. Gelinck, *Adv. Mater.* **2010**, *22*, 4612.
[8] J.-F. Chang, T. Sakanoue, Y. Olivier, T. Uemura, M.-B. Dufourg-Madec, S. G. Yeates, J. Cornil, J. Takeya, A. Troisi, H. Sirringhaus, *Phys. Rev. Lett.* **2011**, *107*, 066601.
[9] D. K. Hwang, C. Fuentes-Hernandez, J. D. Berrigan, Y. Fang, J. Kim, W. J. Potscavage, H. Cheun, K. H. Sandhage, B. Kippelen, *J. Mater. Chem.* **2012**, *22*, 5531.
[10] G. Giri, S. Park, M. Vosgueritchian, M. M. Shulaker, Z. Bao, *Adv. Mater.* **2014**, *26*, 487.
[11] R. Hamilton, J. Smith, S. Ogier, M. Heeney, J. E. Anthony, I. McCulloch, J. Veres, D. D. C. Bradley, T. D. Anthopoulos, *Adv. Mater.* **2009**, *21*, 1166.
[12] N. A. Azarova, J. W. Owen, C. A. McLellan, M. A. Grimminger, E. K. Chapman, J. E. Anthony, O. D. Jurchescu, *Org. Electron.* **2010**, *11*, 1960.
[13] J. Smith, W. Zhang, R. Sougrat, K. Zhao, R. Li, D. Cha, A. Amassian, M. Heeney, I. McCulloch, T. D. Anthopoulos, *Adv. Mater.* **2012**, *24*, 2441.
[14] P. J. Diemer, C. R. Lyle, Y. Mei, C. Sutton, M. M. Payne, J. E. Anthony, V. Coropceanu, J.-L. Brédas, O. D. Jurchescu, *Adv. Mater.* **2013**, *25*, 6956.
[15] W. H. Lee, J. A. Lim, D. Kwak, J. H. Cho, H. S. Lee, H. H. Choi, K. Cho, *Adv. Mater.* **2009**, *21*, 4243.
[16] S. Goffri, C. Müller, N. Stingelin-Stutzmann, D. W. Breiby, C. P. Radano, J. W. Andreasen, R. Thompson, R. A. J. Janssen, M. M. Nielsen, P. Smith, H. Sirringhaus, *Nat. Mater.* **2006**, *5*, 950.
[17] A. C. Arias, F. Endicott, R. A. Street, *Adv. Mater.* **2006**, *18*, 2900.
[18] L. Qiu, J. A. Lim, X. Wang, W. H. Lee, M. Hwang, K. Cho, *Adv. Mater.* **2008**, *20*, 1141.
[19] N. Shin, J. Kang, L. J. Richter, V. M. Prabhu, R. J. Kline, D. A. Fischer, D. M. DeLongchamp, M. F. Toney, S. K. Satija, D. J. Gundlach, B. Purushothaman, J. E. Anthony, D. Y. Yoon, *Adv. Funct. Mater.* **2013**, *23*, 366.
[20] C. Liu, Y. Li, M. V. Lee, A. Kumatani, K. Tsukagoshi, *Phys. Chem. Chem. Phys.* **2013**, *15*, 7917.
[21] J. Smith, R. Hamilton, I. McCulloch, M. Heeney, J. E. Anthony, D. D. C. Bradley, T. D. Anthopoulos, *Synth. Met.* **2009**, *159*, 2365.

[22] J. Kang, N. Shin, D. Y. Jang, V. M. Prabhu, D. Y. Yoon, *J. Am. Chem. Soc.* **2008**, 12273.
[23] J. Smith, R. Hamilton, I. McCulloch, N. Stingelin-Stutzmann, M. Heeney, D. D. C. Bradley, T. D. Anthopoulos, *J. Mater. Chem.* **2010**, *20*, 2562.
[24] D. T. James, B. K. C. Kjellander, W. T. T. Smaal, G. H. Gelinck, C. Combe, I. Mcculloch, R. Wilson, J. H. Burroughes, D. D. C. Bradley, J. Kim, *ACS Nano* **2011**, 9824.
[25] K. Sethuraman, S. Ochiai, K. Kojima, T. Mizutani, *Appl. Phys. Lett.* **2008**, *92*, 183302.
[26] S. H. Kim, S. Nam, J. Jang, K. Hong, C. Yang, D. S. Chung, C. E. Park, W.-S. Choi, *J. Appl. Phys.* **2009**, *105*, 104509.
[27] Y.-H. Kim, Y. U. Lee, J.-I. Han, S.-M. Han, M.-K. Han, *J. Electrochem. Soc.* **2007**, *154*, H995.
[28] J. Kim, J. Jeong, H. D. Cho, C. Lee, S. O. Kim, S.-K. Kwon, Y. Hong, *J. Phys. D. Appl. Phys.* **2009**, *42*, 115107.
[29] S.-I. Shin, J.-H. Kwon, H. Kang, B.-K. Ju, *Semicond. Sci. Technol.* **2008**, *23*, 085009.
[30] S. S. Lee, M. A. Loth, J. E. Anthony, Y.-L. Loo, *J. Am. Chem. Soc.* **2012**, *134*, 5436.